

A DATABASE OF >20 keV ELECTRON GREEN'S FUNCTIONS OF INTERPLANETARY TRANSPORT AT 1 AU

N. AGUEDA¹, R. VAINIO², AND B. SANAHUJA¹

¹ Departament d'Astronomia i Meteorologia, Institut de Ciències del Cosmos, Universitat de Barcelona, Barcelona, Spain

² Department of Physics, University of Helsinki, Helsinki, Finland

Received 2012 April 16; accepted 2012 August 26; published 2012 September 28

ABSTRACT

We use interplanetary transport simulations to compute a database of electron Green's functions, i.e., differential intensities resulting at the spacecraft position from an impulsive injection of energetic (>20 keV) electrons close to the Sun, for a large number of values of two standard interplanetary transport parameters: the scattering mean free path and the solar wind speed. The nominal energy channels of the *ACE*, *STEREO*, and *Wind* spacecraft have been used in the interplanetary transport simulations to conceive a unique tool for the study of near-relativistic electron events observed at 1 AU. In this paper, we quantify the characteristic times of the Green's functions (onset and peak time, rise and decay phase duration) as a function of the interplanetary transport conditions. We use the database to calculate the FWHM of the pitch-angle distributions at different times of the event and under different scattering conditions. This allows us to provide a first quantitative result that can be compared with observations, and to assess the validity of the frequently used term *beam-like* pitch-angle distribution.

Key words: interplanetary medium – methods: numerical – Sun: particle emission

1. INTRODUCTION

Particle experiments on board spacecraft in the heliosphere provide us with in situ measurements of solar energetic particles (SEPs). The measured spectra, time–intensity profiles, and pitch-angle distributions (PADs) play an important role in the investigation of the SEP origin and the properties of their subsequent transport in the interplanetary medium.

SEP time–intensity profiles provide us with information about the temporal evolution of the event (onset time at the spacecraft location, peak time, and duration of the rise and decay phases). Time–intensity profiles that are symmetric with respect to the time of maximum are frequently interpreted as a strong signature of interplanetary scatter-free propagation, while asymmetric profiles are attributed to the effects of interplanetary scattering (see, e.g., Wang et al. 2011). However, it is impossible to untangle the injection history and the interplanetary transport conditions of SEPs observed in situ from the time–intensity profiles alone. The evolution of the particle angular distributions contains information about the relative roles of these two processes, and thus, measured PADs are crucial for our understanding of SEP origin and interplanetary transport.

The term “beam-like PAD” has been frequently used in the analysis of SEP observations to identify scatter-free SEP events. However, it has also been used when the width of the PADs was too large ($\sim 50^\circ$) to reflect interplanetary scatter-free propagation (see, e.g., Figure 10 in Maia et al. 2001).

Haggerty & Roelof (2002) and Haggerty et al. (2003) presented a list of a total of 113 impulsive near-relativistic (38–315 keV) electron events observed between 1997 and 2002 near 1 AU by the *Advanced Composition Explorer* (*ACE*) spacecraft. Haggerty & Roelof (2002) classified these events as scatter-free due to the beam-like, field-aligned PADs observed during the rise phase of the events. As an example, they showed the PAD observed at the peak of the 2000 February 18 electron event. The width of the PAD at half-maximum (33°) was comparable to the opening angle of the collimator (24°), leading Haggerty & Roelof (2002) to suggest that the actual width of the PAD could be unresolved (the beam could be even narrower), suggesting scatter-free interplanetary electron transport. The

authors, however, did not quantify the width of the PADs observed for each event in their list and recent modeling efforts revealed considerable scattering for some of them (see Agueda et al. 2009a). The list of beam-like electron events (extended through 2005 November) is currently available through the *ACE* Science Center Web site.³

In this paper, we use an interplanetary transport model to generate a database of simulation results that can be compared with spacecraft observations in the analysis of near-relativistic electron events. The results are expressed in terms of Green's functions of interplanetary transport, i.e., intensities resulting at the spacecraft position from an impulsive injection of SEPs near the Sun. These tabulated functions—intensities as a function of time, energy, and pitch angle—have been calculated for a large number of values of the standard interplanetary transport parameters.

SEPServer,⁴ a three-year collaborative project funded by the Seventh Framework Programme (FP7-SPACE) of the European Union, aims to build an Internet server with in situ measurements of SEPs and associated electromagnetic emissions. SEPServer will also provide registered users access to the database of electron Green's functions presented in this paper.

In Section 2, we briefly describe the interplanetary transport model used to generate the database of electron Green's functions. In Section 3, we detail the assumed grid of input model parameters. In Section 4, we use the database to quantify the characteristic times of impulsive electron events (onset time, peak time, rise and decay phase duration) as well as the width of the PADs under a variety of interplanetary transport conditions. The goal is to offer the first quantitative measure of these quantities and set a bound on scatter-free transport conditions. We discuss the results in Section 5 and give some examples where the results of this study could be applied. We summarize this work in Section 6.

³ List of beam-like electron events as observed by the *ACE*/EPAM instrument: <http://www.srl.caltech.edu/ACE/ASC/DATA/level3/epam/BeamElectronEvents.pdf>

⁴ <http://www.sepserver.eu/>

2. INTERPLANETARY TRANSPORT MODEL

In the absence of large-scale disturbances, the interplanetary magnetic field (IMF) can be described by a smooth average field, represented by an Archimedean spiral, with a superposed turbulent component. In this case, the propagation of charged particles along the IMF has two components: adiabatic motion along the smooth field and pitch-angle scattering caused by magnetic irregularities. The focused transport equation (Roelof 1969) governs the evolution of the particle's phase space density, $f(s, \mu, t)$,

$$\frac{\partial f}{\partial t} + \mu v \frac{\partial f}{\partial s} + \frac{1 - \mu^2}{2L} v \frac{\partial f}{\partial \mu} - \frac{\partial}{\partial \mu} \left(D_{\mu\mu}(\mu) \frac{\partial f}{\partial \mu} \right) = q(s, \mu, t), \quad (1)$$

where s is the distance along the magnetic field line, μ is the particle pitch-angle cosine, and t is the time. The IMF systematic effect is characterized by the focusing length $L(s) = B(s)/(-\partial B/\partial s)$ in the diverging magnetic field B , and the stochastic forces are described by the pitch-angle diffusion coefficient $D_{\mu\mu}$. The injection of particles from a fixed source close to the Sun is given by $q(s, \mu, t)$. As analytical solutions of Equation (1) are not known, numerical methods need to be applied.

We use an interplanetary transport model to simulate the propagation of solar electrons along the IMF (Agueda et al. 2008). The model uses the Monte Carlo technique to solve the focused transport equation, including the effects of particle streaming along the magnetic field lines, adiabatic focusing by the diverging magnetic field (Roelof 1969), interplanetary scattering by magnetic fluctuations frozen into the solar wind (Jokipii 1966; Dröge 2003), convection with scattering fluctuations, and adiabatic deceleration resulting from the interplay of scattering and focusing (Ruffolo 1995; Kocharov et al. 1998). The model computes the directional distribution of electrons at the spacecraft location resulting from an instantaneous injection at $t = 0$ close to the Sun, i.e., it provides the Green's function of interplanetary transport.

In the initial condition, electrons are released isotropically at a radial distance of two solar radii from the center of the Sun, following a power law in energy ($dN/dE \propto E^{-\gamma}$) in the energy range 24–400 keV, with a spectral index γ . The IMF is described as a smooth average field, represented by an Archimedean spiral for a given solar wind speed, u , with a superposed turbulent component.

The “standard model” of energetic charged-particle scattering (Jokipii 1966; Jaekel & Schlickeiser 1992) predicts a pitch-angle diffusion coefficient of the form

$$D_{\mu\mu} = \frac{1}{2} v(\mu)(1 - \mu^2), \quad (2)$$

where $\mu = \cos \alpha$ is the particle pitch-angle cosine, v is the scattering frequency $v(\mu) = v_0 |\mu|^{q-1}$, and q is the spectral slope of the magnetic field power spectrum. For practical purposes, a pitch-angle diffusion coefficient that resembles the result of the standard theory is often assumed; for example, assuming a scattering frequency of the form $v(\mu) = v_0((|\mu|/1 + |\mu|) + \epsilon)$ (Agueda et al. 2008), ϵ is a parameter that allows us to consider a range of scattering conditions (see Figure 1). In this case, the form of the pitch-angle diffusion coefficient features reduced but finite scattering through $\mu = 0$, as predicted by current models of particle scattering (Dröge 2000). For a number of parameters, the two models can be shown to be almost equivalent; for

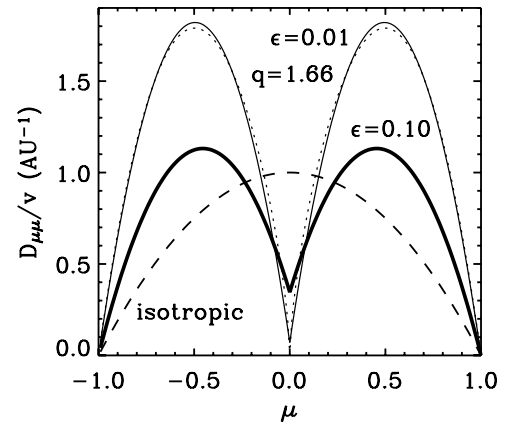


Figure 1. Pitch-angle diffusion coefficients for $\lambda_r = 0.5$ AU; isotropic (dashed curve) and pitch-angle-dependent cases with $\epsilon = 0.10$ (thick curve), $\epsilon = 0.01$ (thin curve), and $q = 1.66$ (dotted curve).

example, they give very similar results for $q = 1.66$ and $\epsilon = 0.01$.

Under strong scattering conditions, the relation of $D_{\mu\mu}$ to the parallel scattering mean free path, λ_{\parallel} , is given by (Hasselmann & Wibberenz 1970)

$$\lambda_{\parallel} = \frac{3v}{8} \int_{-1}^1 \frac{(1 - \mu^2)^2}{D_{\mu\mu}} d\mu = \frac{3v}{4} \int_{-1}^1 \frac{1 - \mu^2}{v(\mu)} d\mu. \quad (3)$$

The mean free path is a convenient parameter to characterize the degree of pitch-angle scattering even when λ_{\parallel} adopts values close to or larger than the observer's distance from the Sun. Based on previous works (e.g., Kallenrode et al. 1992), we assume that it is a good approximation to take the electron radial mean free path, λ_r , to be spatially constant and independent of energy. Then, the mean free path parallel to the IMF line is given by $\lambda_{\parallel} = \lambda_r \sec^2 \psi$, where ψ is the angle between the field line and the radial direction. For a given functional form of the pitch-angle diffusion coefficient, the radial mean free path, λ_r , is the parameter that allows us to describe the degree of pitch-angle scattering processes undergone by electrons.

In a Monte Carlo simulation, quantities of interest are formed by collecting the statistics of the individual simulated particles. In our model, the method of registration consists of counting particles when they are within the interval $r \in [r_{\oplus} - \Delta r/2, r_{\oplus} + \Delta r/2]$. This means that we consider a volume $\sigma(r_{\oplus}) \sec \psi \Delta r$ around the point of observation r_{\oplus} , where $\sigma(r)$ is the cross-sectional area of the flux tube ($\propto B^{-1} \propto r^2 \cos \psi$). We take the flux tube cross-section as $\sigma(r) = r^2 \cos \psi$ corresponding to a flux tube with a 1 sr solid angle at the solar surface. Hence, we derive the near-spacecraft differential intensities, i.e., the number of particles per unit time, unit energy, unit solid angle, and unit area, normalized to one particle injected per steradian at the solar surface.

Since the aim is to compare the simulation results with spacecraft observations, the energy channels and the temporal resolution were chosen in accordance with the observational data to be compared. The pitch-angle cosine was binned in several bins to accomplish an accurate resolution in the PADs.

3. DATABASE OF GREEN'S FUNCTIONS OF INTERPLANETARY TRANSPORT

We used the transport model described in Section 2 to generate a database of Green's functions of interplanetary transport

Table 1
Resolution of the Registration Bins of the Database of the Electron Green's Functions of Interplanetary Transport

Resolution	Spacecraft		
	<i>Wind</i>	<i>ACE</i>	<i>STEREO</i>
Time (minutes)	1	1	1
Pitch angle (°)	22.5	9	9
Energy (keV)	24–30	45–62	45–65
	30–50	62–102	65–105
	50–82	102–175	145–225
	82–135	175–312	255–375
	135–230		
	230–400		

of energetic (>20 keV) electrons. The database calculation was performed using the *Prades* High Performance Computing server at the Centre de Serveis Científics i Acadèmics de Catalunya (CESCA).⁵ It is a Bull NovaScale cluster with 240 cores and an estimated maximum performance of $3.19 \text{ Tflop s}^{-1}$. A total of 40,000 computing hours were required to generate the whole database.

The database of Green's functions was calculated with a time resolution of 1 minute. We assumed the energy bins according to the resolution of three spacecraft located near 1 AU: *ACE*, *STEREO*, and *Wind*. We assumed the energy channels of the LEFS60 telescope of *ACE/EPAM* (Gold et al. 1998), the SST telescope of *Wind/3DP* (Lin et al. 1995), and the SEPT telescope of *STEREO/IMPACT* (Müller-Mellin et al. 2008); see details in Table 1.

The particle experiments on board *ACE* and *Wind* use the rotation of the spacecraft to measure the PADs of SEPs in interplanetary space because it allows a single detector to scan different directions of space as the spacecraft spins. The swath of space swept out by a detector during a spin is normally divided into nearly equally spaced sectors. The number of counts recorded while scanning each sector, together with the measurement of the IMF direction, is used to infer the PADs of the particles (Sanderson et al. 1985). The number of sectors determines the resolution in sampling the directional distribution of the incoming particle population.

The LEFS60 telescope on board *ACE* consists of a detector with a full-cone opening angle of 53° pointing 60° away from the spacecraft spin axis. As the spacecraft spins, the measurements are divided into eight sectors, each 45° wide (Gold et al. 1998). The pitch-angle coverage provided by this telescope varies with the orientation of the magnetic field vector (Agueda et al. 2009b), providing a complete coverage only for a magnetic field vector perpendicular to the spin axis.

Wind/3DP uses five detectors with a full-cone opening angle of 36° mounted at different positions with respect to the spin axis to obtain a complete 4π angular coverage (Lin et al. 1995). Each detector scans a solid angle that is divided into a different

number of sectors. For example, the solid angle scanned by the detector pointing 90° away from the spin axis (in the ecliptic plane) is divided into 16 sectors (22.5° wide), while for the detectors at $18^\circ/162^\circ$, the solid angle is split into only four sectors (90° wide). In total, *Wind/3DP* collects information from 40 different sectors and the data are used to calculate the resulting PAD with a resolution of 22.5° in pitch angle.

On the other hand, the SEPT telescope on board *STEREO* obtains information about the directional distribution of the particles using four static fields of view because the spacecraft is a three-axis stabilized spacecraft. Each field of view has an opening angle of 60° (Müller-Mellin et al. 2008).

In the database of electron Green's functions, the pitch-angle resolution was taken to be 22.5° for *Wind/3DP*, and 9° for *ACE/EPAM* and *STEREO/SEPT*. The angular resolution of these latter two experiments is lower than 9° . However, in the simulations, we chose this higher pitch-angle resolution in order to accomplish an accurate modeling in the case of varying sector/field-of-view orientation, due to fluctuations of the IMF vector. The directions scanned by each sector/field-of-view and their relative probability can be estimated by calculating the angular response of each sector/field-of-view. For example, Agueda et al. (2008) presented a method to calculate the angular response of the sectors scanned by a detector on board a spin-stabilized spacecraft, and recently, Tan et al. (2012) investigated the angular response of the in-ecliptic *Wind/3DP* sectors, covering an approximate solid angle of $22.5^\circ \times 22.5^\circ$.

The database of electron Green's functions was generated for a grid of input parameters. This includes a large number of values of the standard interplanetary transport parameters (see Table 2). We assumed 10 values of the solar wind speed between 300 and 750 km s^{-1} , and 20 values of the electron radial mean free path logarithmically spaced between 0.05 and 1.20 AU. We assumed two different interplanetary pitch-angle diffusion coefficients, isotropic and pitch-angle-dependent with $\epsilon = 0.01$. Finally, we assumed four values of the spectral index of the electron source, between 2.0 and 3.5, with step intervals of 0.5. This makes a database of Green's functions at 1 AU for a total of 1600 different scenarios for three different spacecraft. In each simulation, a total of 10^7 electrons were injected in the energy range 24–400 keV and tracked during a maximum simulation time of 10 hr.

As an example of the Green's functions available in the database, Figure 2 displays the 45–62 keV omnidirectional intensities and the mean pitch-angle cosine evolution for $\lambda_r = 0.10$ AU (left) and $\lambda_r = 1.02$ AU (right), respectively, for $u = 400 \text{ km s}^{-1}$, $\gamma = 3$, and isotropic scattering. The inset plots show the PADs (normalized to maximum) at five different times of the event: two times during the rising phase of the event (1)–(2), at the peak (3), and three times during the event decay phase (4)–(6).

Figure 2 illustrates the dependence of the time–intensity and $\langle \mu \rangle$ profiles on λ_r , as well as how the PAD widths vary. It can be seen that the smaller the value of λ_r , the longer the rise phase of the event and the later and the smaller the peak intensity.

⁵ <http://www.cesca.cat/>

Table 2
Grid of Simulated Parameters in the Electron Database of Green's Functions

Parameters	Range of Values
Spectral index of the source, γ	4 values in [2.0, 3.5], with $\delta\gamma = 0.5$
Solar wind speed, u	10 values in [300, 750] km s^{-1} , with $\delta u = 50 \text{ km s}^{-1}$
Radial mean free path, λ_r	20 values logarithmically spaced between 0.05 and 1.20 AU
Pitch-angle diffusion coefficient, $D_{\mu\mu}$	Isotropic or pitch-angle-dependent ($\epsilon = 0.01$)

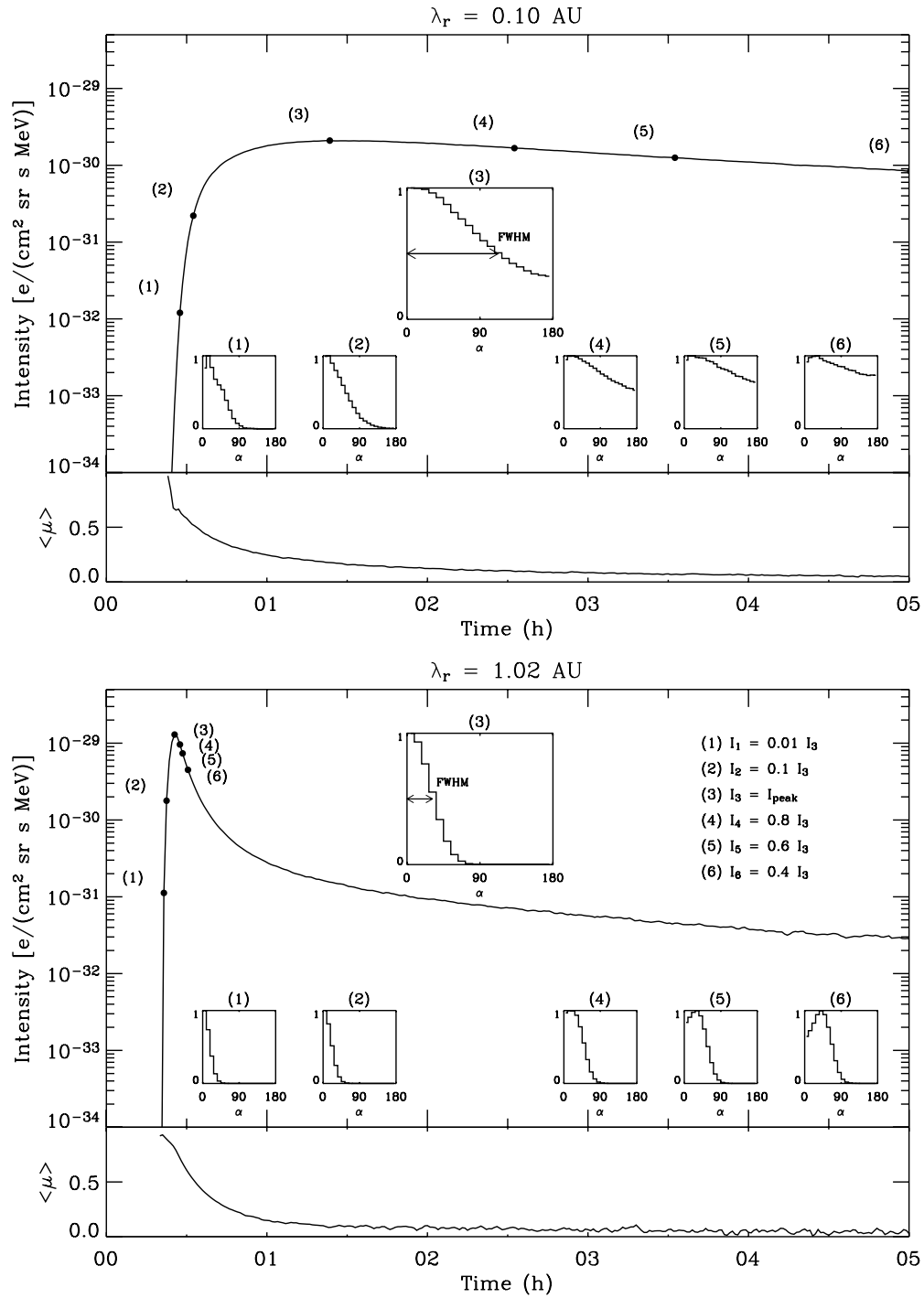


Figure 2. Electron 45–62 keV omnidirectional intensities and mean pitch-angle cosine, $\langle\mu\rangle$, for $\lambda_r = 0.10$ AU (left) and $\lambda_r = 1.02$ AU (right), assuming a solar wind speed of 400 km s^{-1} , isotropic scattering and $\gamma = 3.0$. Intensities are normalized to one particle injected per steradian at the solar surface. The insets in each plot show the normalized PADs at six different intensity levels relative to the event intensity peak, and the FWHM of the PAD at the peak.

Moreover, the FWHM of the PAD at the peak is wider, and the smaller the values of $\langle\mu\rangle$ through the rise phase of the event.

4. PARAMETRIC STUDY

4.1. Characteristic Event Times

For simplicity, from now on, we shall assume a spectral index of the source of 3, a solar wind speed of 400 km s^{-1} , and an isotropic pitch-angle diffusion coefficient.

We define the *onset time* of a given Green's function as the time when the electron intensity is first observed at a

given intensity level, analogous to the observational way of determining the event onset time above the pre-event intensity level.

Points (1) and (2) in Figure 2 show intensity levels of 0.01 and 0.10 relative to the event intensity peak (3), respectively. The onset of the event corresponded to t_1 when the pre-event background was two orders of magnitude smaller than the peak intensity, and to t_2 for a high pre-event intensity level (one order of magnitude smaller) relative to the event intensity peak.

The left panel of Figure 3 shows t_1 as a function of the electron radial mean free path for four energy channels between 45 keV

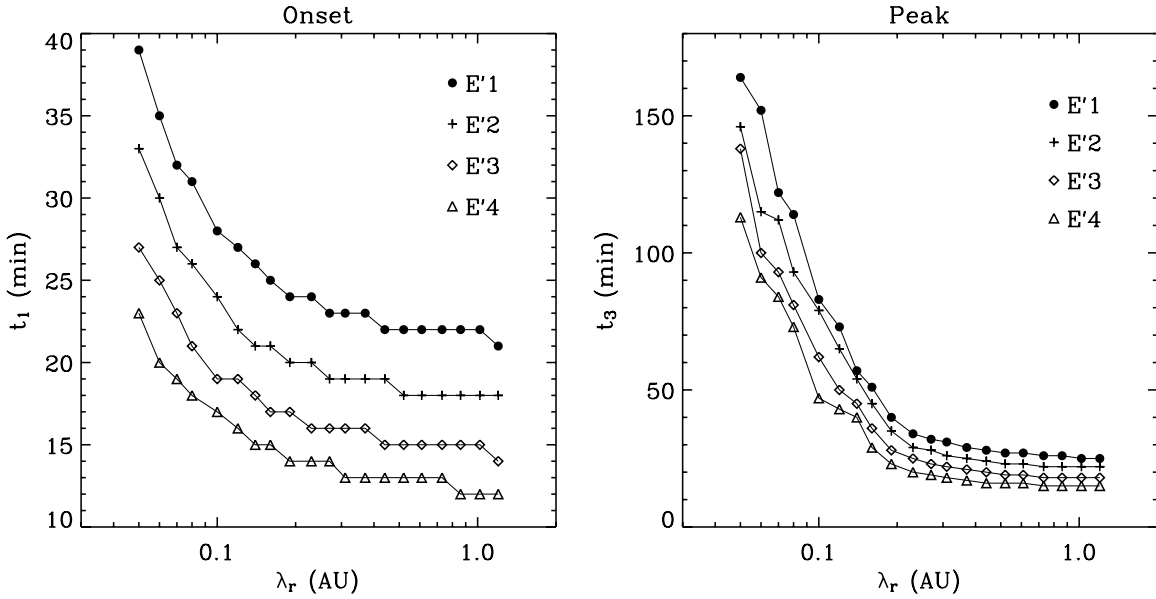


Figure 3. Green's function onset time, t_1 , and peak time, t_3 , for different values of λ_r , assuming an instantaneous injection at $t = 0$, $u = 400 \text{ km s}^{-1}$, isotropic scattering, and $\gamma = 3.0$, for different energy channels (E'1: 45–62 keV; E'2: 62–102 keV; E'3: 102–175 keV; E'4: 175–312 keV). The time resolution of the Green's functions is 1 minute.

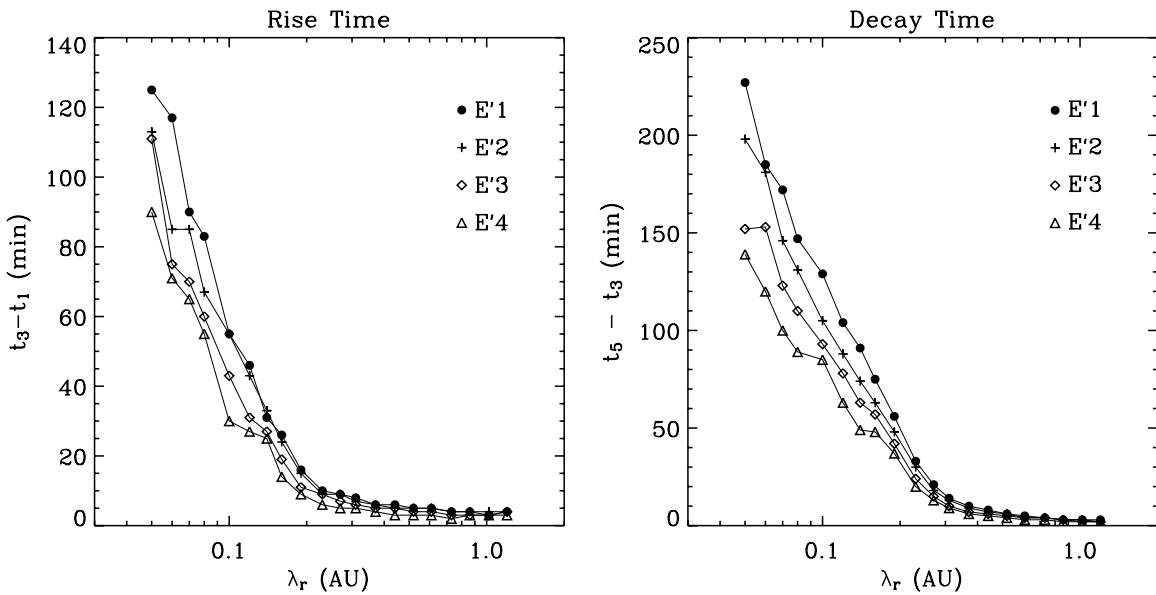


Figure 4. Rise time, $t_3 - t_1$, and decay time, $t_5 - t_3$, as displayed in Figure 3.

and 312 keV. Since the database of Green's functions has a time resolution of 1 minute, the onset time cannot be determined with better accuracy than that. For λ_r values from 0.05 to 1.20 AU, the values of t_1 range between 12 and 23 minutes in the 175–312 keV channel. Thus, interplanetary pitch-angle scattering can delay the onset time by up to 11 minutes (18 minutes for the 45–62 keV channel).

The right panel of Figure 3 shows the peak time, t_3 , of each Green's function for the same range of λ_r values. The peak intensities show clear velocity dispersion at 1 AU under a variety of scattering conditions, and not only for near-scatterer-free propagation to 1 AU. The peak times extend from 15 minutes after injection (for 175–312 keV and $\lambda_r = 1.20$ AU) to 164 minutes (for 45–62 keV and $\lambda_r = 0.05$ AU). The curve is almost flat for $\lambda_r \geq 0.2$ AU, while for $\lambda_r < 0.2$ AU it decreases rapidly. A linear fit to the points in Figure 3 (right panel) yields

$$t_3[\text{minutes}] = -728(\pm 95)\lambda_r[\text{AU}] + 156(\pm 11) \text{ for } \lambda_r \leq 0.2 \text{ AU},$$

$$\text{and } t_3[\text{minutes}] = -6(\pm 1)\lambda_r[\text{AU}] + 26(\pm 1) \text{ for } \lambda_r \geq 0.2 \text{ AU}.$$

We define the rise time of the electron event as the time interval between the onset time and the event intensity peak; that is, $t_3 - t_1$ or $t_3 - t_2$, respectively. Figure 4 (left panel) shows the event rise time ($t_3 - t_1$) for the same λ_r values as in Figure 3. For $\lambda_r = 1.20$ AU, the rise time is 3 minutes at 175–312 keV, while for $\lambda_r = 0.05$ AU it is 90 minutes; values are 4 minutes and 125 minutes at 45–62 keV, respectively.

In order to define the event decay time, we selected three intensity levels after the peak, denoted by (4), (5), and (6) in Figure 2, for relative levels of 0.8, 0.6, and 0.4, respectively—e.g., $I_5 = 0.6I_3$. By calculating $t_j - t_3$, where j can be 4, 5, or 6, one can get an estimation of how fast the omnidirectional intensities decay in each case. The right panel of Figure 4 shows the event decay time ($t_5 - t_3$). For $\lambda_r = 1.20$ AU,

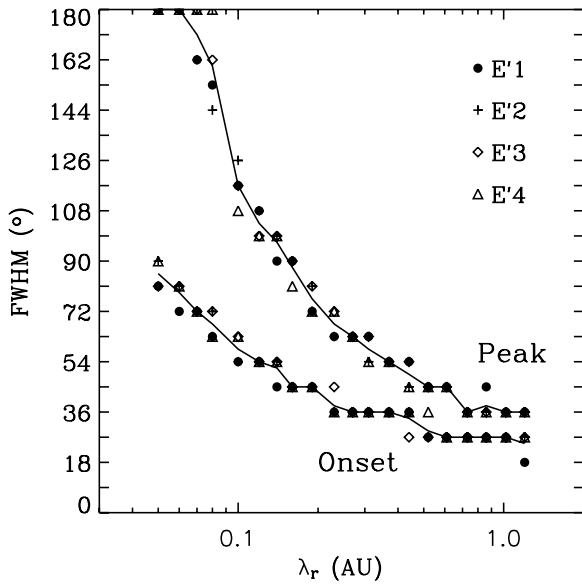


Figure 5. FWHM of the normalized PADs at the onset of the event (t_1) and at the peak (t_3) for different energy channels (E'1: 45–62 keV; E'2: 62–102 keV; E'3: 102–175 keV; E'4: 175–312 keV). The solid curves show the trend averaging over the four energy channels.

it is 2 minutes at 175–312 keV, while for $\lambda_r = 0.05$ AU it is 139 minutes; times are 3 minutes and 227 minutes at 45–62 keV, respectively.

4.2. Width of the Pitch-angle Distributions

Figure 5 shows the FWHM of the simulated PADs at two different times of the event—onset time and peak time—for values of λ_r between 0.05 and 1.20 AU and for different energy channels. It can be seen that the width of the PAD is very similar for different energy channels. This is a consequence of assuming that λ_r is independent of the energy and taking times scaled to the maximum intensity. Table 3 lists the average FWHM of the PAD at the onset (t_1) and at the peak (t_3) for different values of λ_r . At the onset, the width of the PAD takes values between 25° and 86°; at the peak, it ranges from 36° to 180°.

Note that a pitch-angle resolution better than 36° would be necessary to be able to resolve PADs at the peak of the event for $\lambda_r = 1.20$ AU. Since the standard PAD data product provided by *Wind*/3DP has a pitch-angle resolution of 22.5°, the *Wind*/3DP data allow us to distinguish between weak ($\lambda_r = 1.20$ AU) and strong ($\lambda_r = 0.06$ AU) scattering conditions. On the other hand, the telescopes on board *ACE*/EPAM measure SEP distributions in several sectors, with a pitch-angle resolution of 45° at best (corresponding to the case when the magnetic field vector is aligned with the midpoint clock-angle of a sector). For this case, the PADs at the peak would be resolved for $\lambda_r \leq 0.5$ AU. However, the use of the angular response of the sectors allows the estimation of λ_r for larger values. The *STEREO*/SEPT experiment measures electrons through four fields of view with a view cone of 60°. The calculation of the angular response of the four fields of view would be necessary to establish under which IMF conditions the telescope could resolve the PADs for large mean-free paths.

4.3. Other Cases

In the previous sections, we presented a quantitative analysis of the characteristics of the Green's functions for a standard case, assuming that $\gamma = 3.0$, $u = 400$ km s⁻¹, and the pitch-angle scattering is isotropic. One way to study the influence

Table 3
FWHM of the PAD

λ_r (AU)	Onset (°)	Peak (°)
0.06	79	180
0.08	68	160
0.12	54	104
0.16	45	88
0.23	38	68
0.31	36	59
0.44	34	50
0.61	27	45
0.86	27	38
1.20	25	36

of the different input parameters on the characteristics of the Green's functions is to vary one of the parameters at a time and compare those results with the results in Sections 4.1 and 4.2.

If we vary the value of the solar wind speed and assume $u = 600$ km s⁻¹, the length of the IMF Archimedean spiral to 1 AU gets shortened. This translates into values of t_1 and t_3 that are a median of 2 minutes smaller than the ones obtained for the standard case. The mean width of the PADs at the peak shows differences that are smaller than the assumed pitch-angle resolution (9°).

If, instead of varying the value of the solar wind speed, we vary the spectral index of the source and assume that $\gamma = 2.0$, then a flatter electron spectrum is initially injected. This does not modify the onset times of the Green's functions within 1 minute, nor does it modify the time of the peak intensity within 4 minutes. The mean width of the PADs at the peak shows differences that are smaller than the assumed pitch-angle resolution.

Finally, if we assume a pitch-angle-dependent scattering with $\epsilon = 0.01$, and keep the other input parameters as $\gamma = 3.0$ and $u = 400$ km s⁻¹, we obtain an onset time of the event up to 4 minutes later compared to the isotropic case, and the peak intensity is up to 6 minutes later. Note that the scattering frequency ratio between the isotropic and pitch-angle-dependent scattering model depends on μ . The scattering frequency at $\mu = 1$ is 3.5 times larger for a pitch-angle-dependent diffusion coefficient with $\epsilon = 0.01$ than for an isotropic scattering with a constant value of the mean free path (see Figure 1 in Agueda et al. 2010, for more details), while the scattering frequency at $\mu < 0.15$ is smaller than the scattering frequency for isotropic scattering. The larger rate of scattering at small pitch angles is reflected by the wider PADs at the peak of the event, which are 30° wider for $\lambda_r \geq 0.2$ AU for pitch-angle-dependent scattering with $\epsilon = 0.01$.

5. DISCUSSION

The Green's functions of interplanetary transport can be used to deconvolve the interplanetary transport effects from in situ observations (see, e.g., Ruffolo et al. 1998; Agueda et al. 2008). Agueda et al. (2009a) used advanced interplanetary transport modeling to infer the electron injection profile close to the Sun and the electron transport conditions in the heliosphere for a dozen of well-observed near-relativistic electron events. Agueda et al. (2009a) made use of the directional intensities observed in situ by the *ACE* spacecraft, and calculated the angular response of each sector in order to transform the simulated Green's functions into sectorized Green's functions, thus being able to

invert the observations. Proof of the potential of this inverting methodology was provided for *ACE* (Agueda et al. 2009a), *Ulysses* (Agueda et al. 2012), and *Wind* (Malandraki et al. 2012) observations.

Three of the events modeled in Agueda et al. (2009a) appear in the list of beam-like electron events reported by Haggerty & Roelof (2002). These are the events on 2000 May 1, 2002 August 24, and 2004 September 19. Figure 6 shows the 175–312 keV spin-averaged intensity profiles observed on these dates by the LEFS60 telescope aboard *ACE*. The detector points at 60° from the spacecraft’s spin axis and has a full cone opening angle of 53° .

As the spacecraft spins, the measurements are divided into eight sectors, each 45° wide. The directions scanned in a given sector remain constant in the spacecraft coordinate system and their relative probability can be estimated by calculating the angular response of the sector (Agueda et al. 2008). The IMF vector orientation with respect to the spacecraft’s spin axis determines the range in pitch angle seen by the telescope (Agueda et al. 2009b).

The inset plots in Figure 6 show the PAD (normalized to maximum) at the time of the event’s peak intensity. The black dots show the pitch angle measured at the midpoint clock-angle of each sector, and the horizontal bars show the pitch-angle boundaries of each sector. Each plot shows eight data points corresponding to data from the eight LEFS60 sectors. Note that the polarity of the IMF was negative during the 2000 May 1 and the 2002 August 24 events; electrons coming from the Sun along the field lines had $\alpha = 180^\circ$.

The FWHM of the PAD at the peak was 74° for 2000 May 1, 133° for 2002 August 24, and 110° for 2004 September 19, respectively. During the 2000 May 1 event, no antisunward particles propagating along the magnetic field were observed. The pitch-angle coverage at the peak of the event extended over the range $\alpha \in [80^\circ, 160^\circ]$, thus a 20° pitch-angle cone of antisunward particles between 160° and 180° was missed by the telescope. If we assume a flat distribution in the missed antisunward cone, due to normalization to maximum sector intensity, the PAD appears as wide as 74° . One would expect the distribution to be even narrower when normalized to the particle intensities at $\alpha = 180^\circ$.

On the other hand, the pitch-angle coverage was large for the events on 2002 August 24 and 2004 September 19, and only a range of 3° off the magnetic field direction was missed in the antisunward hemisphere of the PAD. Thus, the FWHM of the PAD at the peak is representative of the actual width of the electron distribution. According to Table 3, for widths of 133° and 110° , one would expect λ_r to be shorter than 0.10 AU. Therefore, for these two events, interplanetary scattering played a role in shaping the observed intensities. This is supported by the values of the radial mean free path inferred by Agueda et al. (2009a) for these two events: $\lambda_r = 0.20$ AU and $\lambda_r = 0.16$ AU, respectively. Note that for the event on 2000 May 1, the inferred value of λ_r was much larger (0.90 AU).

Haggerty & Roelof (2002) estimated, for the events in their list, the injection time at the Sun by determining the onset time of the event and shifting it by a transit time of 1.2 AU divided by the highest velocity of the selected channel. The systematic timing disagreement found between electromagnetic emissions and near-relativistic electron injection times led Haggerty & Roelof (2002) to conclude that the electrons released into interplanetary space form a separate population from those electrons generating the prompt flare electromagnetic emission.

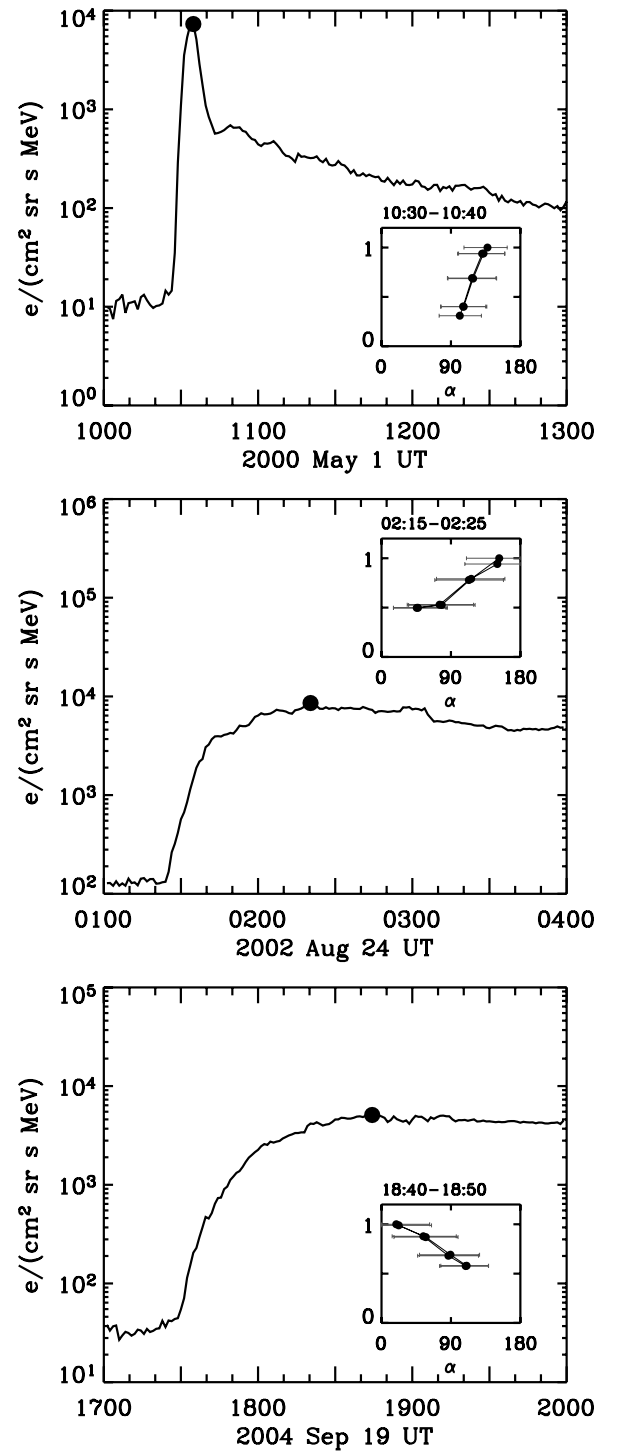


Figure 6. 175–312 keV electron events observed on 2000 May 1, 2002 August 24, and 2004 September 19 by *ACE*. For each event, the inset plot shows the electron PAD normalized to the maximum during a 10 minute accumulation interval at the peak of the event (black dot). The gray horizontal bars mark the pitch-angle range scanned by each sector.

However, interplanetary scattering processes could have played a role in the calculation of such delays, as suggested by Cane (2003).

6. CONCLUSIONS

We used an interplanetary transport model to compute a database of Green’s functions of interplanetary transport

of energetic (>20 keV) electrons at 1 AU. The database includes a total of 1600 different transport scenarios, and it has been found to be applicable to the study of the observations by three spacecraft located near 1 AU: *Wind*, *ACE*, and *STEREO*. The database will be publicly available through the SEPServer Web site and it aims to become a novel tool providing a complementary perspective in the analysis of SEP events.

We quantified the characteristic event times of the Green's functions (onset time, peak time, rise and decay phase duration) under a variety of interplanetary transport conditions. In addition, we provided the first quantitative study of the width of the PADs for different interplanetary transport conditions. The results suggest that a pitch-angle resolution better than 36° is necessary to resolve PADs for a radial mean free path of 1.20 AU.

Our results provide evidence that the term "beam-like PAD" should be used with care, and that observational studies that aim to identify SEP events under weak scattering conditions should provide a quantification of the width of the PADs. We propose a re-visit of the list of beam-like electron events presented by Haggerty & Roelof (2002) specifying, for each event, the PAD width at the peak. This might help to identify some events for which the electron propagation was not effectively identified under weak scattering conditions.

The research leading to these results has received funding from the European Union's Seventh Framework Programme (FP7/2007-2013) under grant agreement No. 262773 (SEPServer). Computational support was provided by the Centre de Serveis Científics i Acadèmics de Catalunya (CESCA). N.A. and B.S. were partially supported by the Ministerio de Economía y Competitividad (Spain), under the project AYA2010-17286. The authors acknowledge support from the

COST Action ES0803 "Developing space weather products and services in Europe."

REFERENCES

- Agueda, N., Lario, D., Ontiveros, V., et al. 2012, *Sol. Phys.*
- Agueda, N., Lario, D., Vainio, R., et al. 2009a, *A&A*, **507**, 981
- Agueda, N., Vainio, R., Lario, D., & Sanahuja, B. 2008, *ApJ*, **675**, 1601
- Agueda, N., Vainio, R., Lario, D., & Sanahuja, B. 2009b, *Adv. Space Res.*, **44**, 794
- Agueda, N., Vainio, R., Lario, D., & Sanahuja, B. 2010, *A&A*, **519**, A36
- Cane, H. V. 2003, *ApJ*, **598**, 1403
- Dröge, W. 2000, *Space Sci. Rev.*, **93**, 121
- Dröge, W. 2003, *ApJ*, **589**, 1027
- Gold, R. E., Krimigis, S. M., Hawkins, S. E., III, et al. 1998, *Space Sci. Rev.*, **86**, 541
- Haggerty, D. K., & Roelof, E. C. 2002, *ApJ*, **579**, 841
- Haggerty, D. K., Roelof, E. C., & Simnett, G. M. 2003, *Adv. Space Res.*, **32**, 2673
- Hasselmann, K., & Wibberenz, G. 1970, *ApJ*, **162**, 1049
- Jaekel, U., & Schlickeiser, R. 1992, *Ann. Geophys.*, **10**, 541
- Jokipii, J. R. 1966, *ApJ*, **146**, 480
- Kallenrode, M.-B., Wibberenz, G., & Hücke, S. 1992, *ApJ*, **394**, 351
- Kocharov, L., Vainio, R., Kovaltsov, G. A., & Torsti, J. 1998, *Sol. Phys.*, **182**, 195
- Lin, R. P., Anderson, K. A., Ashford, S., et al. 1995, *Space Sci. Rev.*, **71**, 125
- Maia, D., Pick, M., Hawkins, S. E., III, Fomichev, V. V., & Jiřička, K. 2001, *Sol. Phys.*, **204**, 197
- Malandraki, O., Agueda, N., Papaioannou, A., et al. 2012, *Sol. Phys.*, in press
- Müller-Mellin, R., Böttcher, S., Falenski, J., et al. 2008, *Space Sci. Rev.*, **136**, 363
- Roelof, E. C. 1969, in *Lectures in High-Energy Astrophysics*, ed. H. Ögelman & J. R. Wayland (Washington, DC: NASA), 111
- Ruffolo, D. 1995, *ApJ*, **442**, 861
- Ruffolo, D., Khumlumert, T., & Youngde, W. 1998, *J. Geophys. Res.*, **103**, 20591
- Sanderson, T. R., Reinhard, R., van Nes, P., & Wenzel, K.-P. 1985, *J. Geophys. Res.*, **90**, 19
- Tan, L. C., Malandraki, O. E., Reames, D. V., et al. 2012, *ApJ*, **750**, 146
- Wang, L., Lin, R. P., & Krucker, S. 2011, *ApJ*, **727**, 121